Ultrafast resonant interatomic Coulombic decay induced by quantum fluid dynamics

A. C. LaForge *et al.*

(Dated: February 16, 2021)

SUPPLEMENTARY NOTE 1: CALCULATION OF He*-He* ICD WIDTHS

The resonant ICD widths were computed with the Fano-Configuration Interaction-Stieltjes (Fano-CI-Stieltjes) method [1] as implemented in the CIPPRES plugin [2] of Quantum Package 2.0 (QP2) [3], [4]. Moreover, we have used the restricted Hartree-Fock molecular orbitals of He_2 constructed from a cc-pVQZ basis set [5] augmented with [6s,6p,6d] diffuse functions of the Kaufmann-Baumeister-Jungen type [6] on each helium center.

SUPPLEMENTARY NOTE 2: He*-He* PAIR POTENTIALS

The He-He (D_{2h} point group) interaction potentials corresponding to 1s2s and 1s2p He atomic asymptotes, shown in Fig. 1 were obtained with equation-of-motion coupled clusters method CC3-EOM level [7, 8] by using the Psi4 code [9]. The basis set used in this calculation was taken from Ref. [10]. The doubly excited He states (He*-He*) correlating with the first excited ^{1}S and ^{3}S atomic asymptotes were computed using the full configuration interaction method as implemented in the DETCI module [11] of Psi4 by solving for the lowest 32 roots in a given irreducible representation and then locating the states according to the correct asymptotic energies. Due to the computational cost, these calculations employed a smaller basis set as described in Refs. [12–14], which can still reproduce the atomic asymptotic energies with sufficient accuracy. All the calculated potentials were corrected for the basis set superposition error by the counterpoise method of Boys and Bernardi [15].
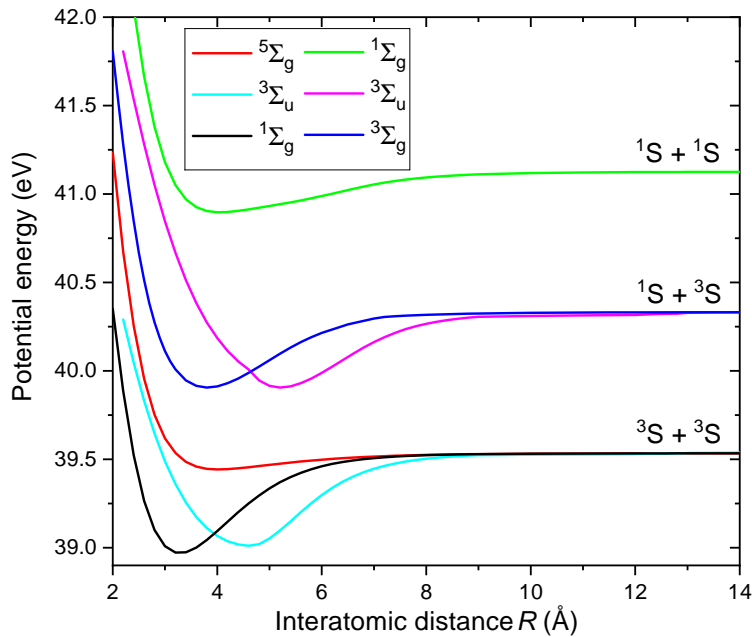
Supplementary Fig. 1. Potential energy curves for two He* atoms excited to their lowest excited states 1s2s ^{1,3}S.

SUPPLEMENTARY NOTE 3: TDDFT SIMULATIONS

The DFT and TDDFT approaches to superfluid liquid He are thoroughly described in Ref. [16], and the dynamic evolution of a single He* bubble in a ^{4}He droplet has been studied in Ref. [17]. The extension to two He* bubbles in bulk superfluid helium proceeds similarly. One singles out two arbitrary points in the superfluid, $\mathbf{r}_X$ and $\mathbf{r}_Y$, where the two excited helium atoms are assumed to be and build the following density:

$$\rho_{d_0}(\mathbf{r}) \equiv \rho_0\, g(|\mathbf{r}_X - \mathbf{r})|)\, g(|\mathbf{r}_Y - \mathbf{r})|)\,, \tag{1}$$

where ρ_0 is the ^{4}He density at $P = T = 0$ ($\rho_0 = 0.0218$ Å^{-3}) and $g(r)$ is the pair distribution function of liquid ^{4}He obtained from QMC calculations [18]. This procedure yields two "atom bubbles" located at the chosen positions $\mathbf{r}_X$ and $\mathbf{r}_Y$. The physical control parameter is the initial distance $d_0 = |\mathbf{r}_X - \mathbf{r}_Y|$. To obtain the wave function $\Phi(\mathbf{r})$ for each of the He* atoms needed to start the dynamics, we have proceeded as in Ref. [17]. We have used TDDFT to address the time evolution of the superfluid [16], to which the two He* atoms are self-consistently coupled. The dynamics are triggered by substituting the Aziz He-He potential [19] used to generate the "static" wave functions $\Phi_X(\mathbf{r})$ and $\Phi_Y(\mathbf{r})$ with the He-He* and He*-He* potentials where He* represents the 1s2s ^{1}S excited state.

We have solved the coupled TDDFT equation for the superfluid and the two Schrödinger equations for the He*s:

$$-i\hbar\frac{\partial}{\partial t}\Psi(\mathbf{r}) = \left\{-\frac{\hbar^2}{2m_{\mathrm{He}}}\nabla^2 - \mu + \int d\mathbf{r}'\,\left[|\Phi_X(\mathbf{r}')|^2 + |\Phi_Y(\mathbf{r}')|^2\right]\,\mathcal{V}_{He-He^*}(|\mathbf{r}' - \mathbf{r})|) + \frac{\delta}{\delta\rho}\mathcal{E}(\rho)\right\}\Psi(\mathbf{r})$$

$$-i\hbar\frac{\partial}{\partial t}\Phi_X(\mathbf{r}) = \left\{-\frac{\hbar^2}{2m_{\mathrm{He}}}\nabla^2 + \int d\mathbf{r}'\,\mathcal{V}_{He-He^*}(|\mathbf{r} - \mathbf{r}'|)\rho(\mathbf{r}') + \int d\mathbf{r}'\,\mathcal{V}_{He^*-He^*}(|\mathbf{r} - \mathbf{r}'|)|\Phi_Y(\mathbf{r}')|^2\right\}\Phi_X(\mathbf{r})$$

$$-i\hbar\frac{\partial}{\partial t}\Phi_Y(\mathbf{r}) = \left\{-\frac{\hbar^2}{2m_{\mathrm{He}}}\nabla^2 + \int d\mathbf{r}'\,\mathcal{V}_{He-He^*}(|\mathbf{r} - \mathbf{r}'|)\rho(\mathbf{r}') + \int d\mathbf{r}'\,\mathcal{V}_{He^*-He^*}(|\mathbf{r} - \mathbf{r}'|)|\Phi_X(\mathbf{r}')|^2\right\}\Phi_Y(\mathbf{r}) \tag{2}$$

where $\mathcal{E}(\rho)$ is the ^{4}He functional of Ref. [20] and $\delta\mathcal{E}/\delta\rho$ is the DFT mean field written in a compact way. The starting configuration at $t = 0$ is the $\rho_{d_0}(\mathbf{r})$ liquid density, Eq. (1), and the wave functions $\Phi_X(\mathbf{r})$ and $\Phi_Y(\mathbf{r})$. Although not necessary in an ideal situation, the chemical potential μ is included because of our way of damping the density waves produced by the expansion of the He* bubbles.

Indeed, during the time evolution of excited impurities in bulk liquid helium, sound waves are released from the surface of the atomic bubble which eventually reach the cell boundary (periodic boundary conditions are imposed). If no action is taken, waves would bounce back and invalidate the simulation. A way to avoid this problem is to include damping in the time-dependent equation governing the helium evolution, first line of Eq. (2), by replacing $i \longrightarrow i + \Lambda(\mathbf{r})$ [21]. This corresponds to a rotation of the time axis in the complex plane by introducing a damping field $\Lambda(\mathbf{r})$:

$$\Lambda(\mathbf{r}) = \Lambda_0 \sum_{i=1,2,3}\left[1 + \tanh\left(\frac{|x_i| - s_{i_0}}{a}\right)\right] \tag{3}$$

The evolution is free of damping $[\Lambda(\mathbf{r}) \ll 1]$ when $|x_i| < s_{i_0} - 2a$. This prescription works extremely well as it efficiently damps the excitations in the helium wave function near the cell boundaries and does not require a large buffer region.

The calculations have been carried out using the 4He-DFT BCN-TLS computer package [22]. We used 256^3 points in the cubic box $-25.6 \leq x_i \leq 25.6$ Å, i. e., $\Delta x_i = 0.2$ Å; s_{i_0} was fixed to 23.6 Å, $a = 2$ Å, and $\Lambda_0 = 2$ (dimensionless). The region in which the absorption potential acts is large enough to accommodate the system under study. The time step for the dynamics are $\Delta t = 0.05$ fs; this is needed to have a good energy conservation and wave function normalization.

SUPPLEMENTARY NOTE 4: ANIMATIONS OF BUBBLE DYNAMICS IN SUPERFLUID HELIUM

The appended animations visualize the dynamics of two excited helium atoms within superfluid helium. When a helium atom is resonantly excited (1s2s state), a void or "bubble" forms around it, resulting in the complete absence of atoms in the surrounding volume [17]. The animations are the result of time-dependent density functional theory (TDDFT) calculations (see Suppl. Note 3) for the case of two excited atoms being placed at distance d from each other. The downloadable animations for $d = 8$ Å, 10 Å, and 15 Å, are 'He-animations-8.0A.mp4', 'He-animations-10.0A.mp4', and 'He-animations-15.0A.mp4', respectively. The ground state atomic density goes from dark purple

to yellow and the excited state atomic density goes from dark green to pink. The three animations show how the dynamics are dependent on the initial distance d. For $d = 8$ Å, the two bubbles quickly (~ 400 fs) merge and the two excited states oscillate in close distance to one another. Similar dynamics are observed for smaller distances d shown in Fig. 4 of the manuscript. For $d = 10$ Å and $d = 15$ Å, the bubbles also merge, but on a longer timescales > 1 ps, and > 10 ps, respectively. In case of a He nanodroplet of the size of few nm, one or both excited atoms would mostly likely be ejected out of the droplet prior to ICD, thus suppressing contributions from slow ICD.

SUPPLEMENTARY NOTE 5: MONTE-CARLO SIMULATIONS

The MC model combines all relevant processes to describe the ICD dynamics in He nanodroplets in one simplified model. It is based on the ICD widths $\Gamma(d)$ (bottom right panel in Fig. 4 of the manuscript), where the distance d between adjacent He* is inferred from the TDDFT simulations as a time-dependent function.

A.   Parameterization of ICD decay widths

$\Gamma(d)$ is given as data points for discrete values of the distance d with 1 Å spacing. To obtain an analytic function used for the MC simulations we have approximated $\Gamma(d)$ by an exponentially decaying function

$$\Gamma_{\mathrm{ICD}}(d) = \begin{cases} 4 \text{ meV,} & \text{if } d < 4 \text{ Å} \\ 4 \exp\left(-\frac{(d-4)}{0.817}\right) \text{ meV,} & \text{if } d \geq 4 \text{ Å} \end{cases} \tag{4}$$

which is constant at short-range $d < 4$ Å. To take into account the contribution of the two spin states 1s2s $^{1,3}S$ of He*, we averaged the spin contributions according to random spin orientation. The resulting function is only valid at intermediate distances, where the ICD width depends exponentially on d. Although for larger distances, Eq. (4) does not give reliable results, the accuracy of our simulation remains unaffected as the ICD time exceeds 100 ps already at $d = 10$ Å. Thus, the contribution of Γ at large $d > 10$ Å is completely negligible for the experimentally observed timescales.

B.   Simulation of partially excited He droplets

As a next step, we modeled a He droplet with N He atoms as a homogeneous sphere with a density of 22 atoms/nm^3. The atoms are approximated as hard spheres, corresponding to a pair-distribution function

$$\rho_{\mathrm{He}}(d) = \begin{cases} 0, & \text{if } d < 3.58 \text{ Å} \\ \rho_0, & \text{if } d \geq 3.58 \text{ Å.} \end{cases} \tag{5}$$

The positions of excited He atoms in the droplet are chosen at random according to the excitation probability calculated from the experimental parameters. For this, we assumed the photoexcitation cross section at $h\nu = 21.6$ eV (1s2p droplet band) to be 25 Mb [23, 24] and the FEL pulse to be a delta function in time. Subsequently, all possible pairwise interactions between He* are identified and binned according to their initial distances d_0. The bin size is determined by the available TDDFT simulations. The systematic error on the time-dependent distances $d(t)$ resulting from the binning can be estimated from the TDDFT simulations. All initial distances $d_0 \leq 9$ Å converge to the same minimum value within 400 fs, and the possible uncertainty from the bin size is smaller than the time resolution of our experiment. For the larger distances, we saw that differences $\Delta d < 1$ Å in d_0 have a large impact on $d(t)$. We have refrained from trying to do a functional approximation of the time-distance behavior due to the rather complex dynamics and the minor impact on the observed behavior. A more accurate determination of the trajectories in the transition region would require a dense set of TDDFT simulations which would represent a tremendous computational effort.

The ensemble of He* is then propagated in time with a step size of 500 as. During the time propagation, the pairwise interactions are treated independently of each other, neglecting any many-body effects with more than two participants. For each time step, the ICD probability for each pairwise interaction is calculated as $\Gamma(d(t))$ according to the $d(t)$ trajectory corresponding to the d_0 bin. Additionally, the UV-probe laser is implemented as a Gaussian pulse with a width corresponding to the full width of the measured XUV-UV cross correlation. He* that undergo ICD,

or are ionized by the probe laser, are counted and removed from the calculation including all pairwise interactions these excitations participated in. Any impact of the created ions on the remaining excitations is neglected. The total time propagation is done up to 100 ps after the FEL pulse. The step size of 500 as was chosen in order to satisfy the condition $\Delta N \ll N$, *i. e.* that in each time step, the change in total population is close to zero.

Each simulation creates one data set for a fixed pump-probe delay, droplet size, and excitation density. To acquire a sufficiently converged result for the ICD electron and photoelectron counts, we simulated up to 10^4 droplets for each parameter set. To get a time-dependent ICD curve, we have repeated the simulation for each pump-probe delay. All data points created for one parameter set at different pump-probe delays form a time-dependent ICD curve as displayed in Fig. 7 b) of the manuscript.

C. Finite size effects and ejection of He*

Due to the finite size of the He droplets and the repulsive forces acting on excited He atoms in the droplet, ejection of He* out of the droplets is a competing process. He* ejection has previously been investigated and, here, we will focus on the implementation of the previous results [17]. In our simulation, a hard-cutoff ejection mechanism is adopted by deleting all pairwise interactions of those He* that satisfy the conditions of being close to the droplet surface ($d_s < 7.5$ Å) and not having another He* nearby ($d_0 > 9.5$ Å). Neglecting ejection of He* for large initial separation from the surface is a reasonable approximation in view of the short time scale of the experiment (less than 10 ps) [17]. Photoionization of the ejected He* is still possible and taken into account. The choice of these values, and their impact on the simulations will be discussed below.
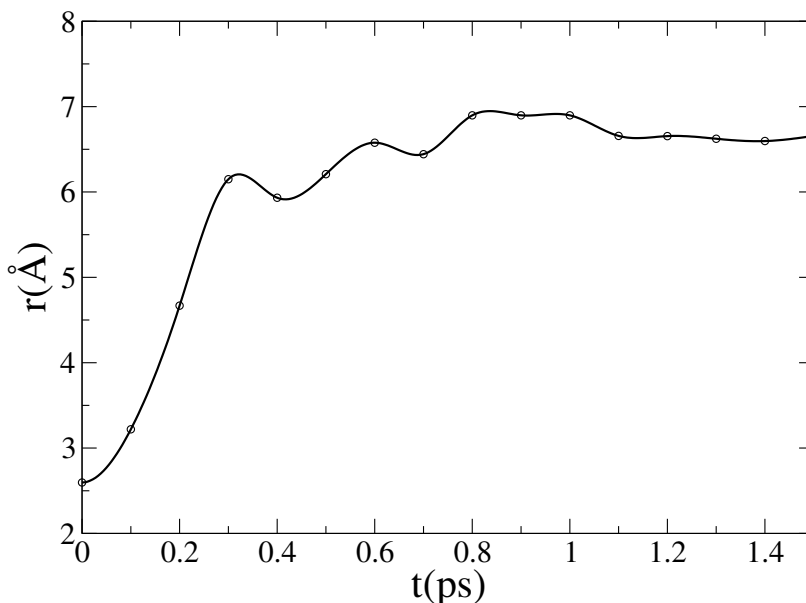
Supplementary Fig. 2. Evolution of the radius of a bubble forming around a He* in bulk superfluid helium as obtained from TDDFT simulations.

When multiple excitations are present in the droplet, the ejection process is more complex, depending on the geometry and exact positions of the excitations. Furthermore, as observed in the lower left panel of Fig. 4 of the manuscript, shock waves play an important role in the trajectories of He*. However, in a first approximation we have neglected all geometric effects and simply look at the basic dynamics of bubble formation. Supplementary Fig. 2 shows the expulsion of the He density around a He* in a time-resolved way, from which we have extracted two relevant parameters: The bubble expands within about 500 fs and reaches a final radius of roughly 7 Å. Considering the dynamics from the TDDFT simulations and taking the previously measured desorption dynamics [17] into account, we identify two critical cases. If two He*s are closer to one another than 10 Å, the merging of the bubbles happens during the first expansion phase of the bubbles within 500 fs. In this case, none of the excitations will leave the droplet as free atoms, independent of their distance from the droplet surface. The second critical case is defined by the initial distance to the next He* being larger than 10 Å. In this case, the merging will be slightly delayed since at

first, the two bubbles repel each other via shockwaves. If one of the He* is close enough to the droplet surface that the expanding bubble breaks the surface, the He* is most likely ejected before bubble merging. According to these two critical cases, the limits for ejection given in the manuscript were chosen. The good agreement with the experimental data indicates that this approach is a reasonable approximation for this complex system. A more rigorous treatment would require us to take different initial geometries into account and to carry out full TDDFT simulations for each of them, which is far beyond our possibilities.

D. Rate equation model for resonant ICD in He droplets

Chemical reactions described by chemical kinetics are usually diffusion limited and barrier activation controlled, i. e. the reaction constant depends on relative Brownian velocity of the reactants, which is large compared to mean distance between participants and the reaction time. In our case of ICD of He*s in He droplets, the diffusive motion of the participants is slow compared to the observed ICD reaction rate. However, the rate constant depends on the distance between the active particles rather than their relative speeds. To benchmark our MC simulation against the simplest possible model which assumes stationary positions of the He* in the droplet, we have developed a simple rate equation model based on distance-dependent ICD widths $\Gamma(d)$.

If several He atoms in a droplet are excited, the total number of pairwise interactions is $N(N-1)/2$, where N is the number of He*. In our case, the calculated decay widths drop exponentially with increasing d. Thus, we can make the approximation that ICD happens exclusively between nearest-neighbors. Formally, this approximation holds if the pairwise decay width decreases with distance d according to $\Gamma(d) = d^{-x}$ with $x > 3$, since for $x \leq 3$ the integral interaction strength for a single He* with all surrounding He*s,

$$\int_0^\infty 4\pi d^2 \Gamma(d)\, \mathrm{d}d, \tag{6}$$

diverges. In this nearest neighbor approximation, the product of the volume element times the interaction strength, $4\pi d^2 \Gamma(d)$ drops substantially when increasing d from nearest-neighbor to next-to-nearest-neighbor distance and thus ICD predominantly occurs for pairs of nearest neighbors. This approximation can be viewed as replacing the initial population N of He* by $N/2$ pairs of He* which decay according to a linear rate equation,

$$\frac{\mathrm{d}\rho(t)}{\mathrm{d}t} = -k\rho(t). \tag{7}$$

Here, the rate constant $k = \tau^{-1} = \Gamma e/\hbar$, where e is the elementary charge and $\hbar$ is the reduced Planck constant. The distance dependence of the rate constant $k(d)$ should then be included in the rate equation for an ensemble of He* by integrating over distances d,

$$\frac{\mathrm{d}\rho(t)}{\mathrm{d}t} = -\int_0^\infty k(d)\rho_d(t)\, \mathrm{d}d. \tag{8}$$

Here, $\rho_d(t)$ is the density of He* pairs per unit distance. The solution of this rate equation is

$$\rho(t) = \int_0^\infty \rho_{d,0} \exp(-k(d)t)\, \mathrm{d}d. \tag{9}$$

This function describes a superposition of exponential decay functions with different time constants. The differential initial He* density $\rho_{d,0}$ takes the role of a weighting factor accounting for the distribution of initial nearest-neighbor distances. Fig. 8 a) in the manuscript illustrates this function for different excitation probabilities p_{exc} as blue lines. For comparison, the full dynamical model (red) and the experimental data (black squares) are additionally shown. We see that the time behavior of the linear rate-equation model assuming fixed He* positions significantly differs from the experimentally observed ones. The ICD depletion decays non-exponentially and much more slowly than the experimental data and the dynamical simulation. Furthermore, the observed timescales drastically change when varying the excitation probability, in contrast to the experimental findings shown in Fig. 3 a) of the manuscript. Fig. 8 b) in the manuscript shows the normalized $\rho_{d,0}$ binned into three different intervals of $\tau(d)$. For high excitation probability $\gtrsim 2\,\%$, contributions to the initial He* population with short ICD times $\tau < 5$ ps dominates. However, for all excitation probabilities used in the experiment ($p_{\mathrm{exc}} < 1\,\%$), the dominant contributions have $\tau > 100$ ps. This

highlights the importance of atomic motion for the effective ICD dynamics and efficiency, which in the particular case of He nanodroplets is given by the peculiar evolution of He* bubbles.

———————

[1] Tsveta Miteva, Sévan Kazandjian, and Nicolas Sisourat, "On the computations of decay widths of fano resonances," Chem. Phys. **482**, 208–215 (2017).

[2] "Github website," `https://github.com/sisourat/qp2_plugins_nsisourat`, [Accessed: 10-October-2017].

[3] Yann Garniron, Thomas Applencourt, Kevin Gasperich, Anouar Benali, Anthony Ferté, Julien Paquier, Barthélémy Pradines, Roland Assaraf, Peter Reinhardt, Julien Toulouse, *et al.*, "Quantum package 2.0: An open-source determinant-driven suite of programs," J. Chem. Theory Comput. **15**, 3591–3609 (2019).

[4] *See also* `https://quantum-package.readthedocs.io/en/master/`.

[5] David E Woon and Thom H Dunning Jr, "Gaussian basis sets for use in correlated molecular calculations. iv. calculation of static electrical response properties," J. Chem. Phys. **100**, 2975–2988 (1994).

[6] K Kaufmann, W Baumeister, and M Jungen, "Universal gaussian basis sets for an optimum representation of Rydberg and continuum wavefunctions," J. Phys. B **22**, 2223 (1989).

[7] Henrik Koch, Ove Christiansen, Poul J ørgensen, Alfredo M Sanchez de Merás, and Trygve Helgaker, "The cc3 model: An iterative coupled cluster approach including connected triples," J. Chem. Phys. **106**, 1808–1818 (1997).

[8] Christopher E Smith, Rollin A King, and T Daniel Crawford, "Coupled cluster methods including triple excitations for excited states of radicals," J. Chem. Phys. **122**, 054110 (2005).

[9] Justin M Turney, Andrew C Simmonett, Robert M Parrish, Edward G Hohenstein, Francesco A Evangelista, Justin T Fermann, Benjamin J Mintz, Lori A Burns, Jeremiah J Wilke, Micah L Abrams, *et al.*, "Psi4: an open-source ab initio electronic structure program," Wiley Interdiscip. Rev. Comput. Mol. Sci. **2**, 556–565 (2012).

[10] Steven L Fiedler and Jussi Eloranta, "Interaction of helium Rydberg state atoms with superfluid helium," J. Low Temp. Phys. **174**, 269–283 (2014).

[11] C David Sherrill and Henry F Schaefer III, "The configuration interaction method: Advances in highly correlated approaches," *Adv. Quantum Chem., volume=34, pages=143–269, year=1999, publisher=Elsevier*, .

[12] KK Sunil, J Lin, H Siddiqui, PE Siska, KD Jordan, and Ron Shepard, "Theoretical investigation of the a 3σ+ u, a 1σ+ u, c 3σ+ g, and c 1σ+ g potential energy curves of he2 and of he*(2 1 s, 2 3 s)+ he scattering," J. Chem. Phys. **78**, 6190–6202 (1983).

[13] Cary F Chabalowski, James O Jensen, David R Yarkony, and Byron H Lengsfield III, "Theoretical study of the radiative lifetime for the spin-forbidden transition a 3σ+ u→ x 1σ+ g in he2," J. Chem. Phys. **90**, 2504–2512 (1989).

[14] J Eloranta and VA Apkarian, "The triplet he 2* Rydberg states and their interaction potentials with ground state he atoms," J. Chem. Phys. **115**, 752–760 (2001).

[15] S F Boys and FJMP Bernardi, "The calculation of small molecular interactions by the differences of separate total energies. some procedures with reduced errors," Mol. Phys. **19**, 553–566 (1970).

[16] Francesco Ancilotto, Manuel Barranco, François Coppens, Jussi Eloranta, Nadine Halberstadt, Alberto Hernando, David Mateo, and Marti Pi, "Density functional theory of doped superfluid liquid helium and nanodroplets," Int. Rev. Phys. Chem. **36**, 621–707 (2017).

[17] M Mudrich, AC LaForge, A Ciavardini, P O'Keeffe, C Callegari, M Coreno, A Demidovich, M Devetta, M Di Fraia, M Drabbels, *et al.*, "Ultrafast relaxation of photoexcited superfluid he nanodroplets," Nat. Commun. **11** (2020).

[18] J Boronat and J Casulleras, "Monte carlo analysis of an interatomic potential for he," Phys. Rev. B **49**, 8920 (1994).

[19] Ronald A Aziz, Frederick RW McCourt, and Clement CK Wong, "A new determination of the ground state interatomic potential for he2," Mol. Phys. **61**, 1487–1511 (1987).

[20] Francesco Ancilotto, M Barranco, F Caupin, R Mayol, and M Pi, "Freezing of he 4 and its liquid-solid interface from density functional theory," Phys. Rev. B **72**, 214522 (2005).

[21] David Mateo, Dafei Jin, Manuel Barranco, and Martí Pi, "Excited electron-bubble states in superfluid 4he: A time-dependent density functional approach," J. Chem. Phys. **134**, 044507 (2011).

[22] M. Pi, F. Ancilotto, F. Coppens, N. Halberstadt, A. Hernando, A. Leal, D. Mateo, R. Mayol, and M. Barranco, "^{4}He-DFT BCN-TLS: A Computer Package for Simulating Structural Properties and Dynamics of Doped Liquid Helium-4 Systems. https://github.com/bcntls2016/," `https://github.com/bcntls2016/` (2017).

[23] D Buchta, Siva Rama Krishnan, Nils Benedict Brauer, Marcel Drabbels, P O'Keeffe, M Devetta, Michele Di Fraia, C Callegari, R Richter, M Coreno, *et al.*, "Extreme ultraviolet ionization of pure he nanodroplets: Mass-correlated photoelectron imaging, penning ionization, and electron energy-loss spectra," J. Chem. Phys. **139**, 084301 (2013).

[24] Y Ovcharenko, V Lyamayev, R Katzy, M Devetta, A LaForge, P O'Keeffe, O Plekan, P Finetti, Michele Di Fraia, M Mudrich, *et al.*, "Novel collective autoionization process observed in electron spectra of he clusters," Phys. Rev. Lett. **112**, 073401 (2014).